Front. Mech. Eng.
https://doi.org/10.1007/s11465-020-0622-2

RESEARCH ARTICLE

Qiang GAO, Yuchuan ZHU, Changwen WU, Yulei JIANG

Development of a novel two-stage proportional valve with a pilot digital flow distribution

Abstract Pilot two-stage proportional valves are widely used in high-power hydraulic systems. For the purpose of improving the dynamic performance, reliability, and digitization of the traditional proportional valve, a novel two-stage proportional valve with a pilot digital flow distribution is proposed from the viewpoint of the dual nozzle-flapper valve's working principle. In particular, the dual nozzle-flapper is decoupled by two high-speed on/off valves (HSVs). First, the working principle and mathematical model of the proposed valve are determined. Then, the influences of the control parameters (duty cycle and switching frequency) and structural parameters (fixed orifice's diameter and main valve's spring) on the main valve's motion are analyzed on the basis of theory, simulation, and experiment. In addition, in optimizing the value of the fixed orifice's diameter, a new design criterion that considers the maximum pressure sensitivity, flow controllability, and flow linearization is proposed to improve the balance between the effective displacement and the displacement fluctuation of the main valve. The new scheme is verified by simulations and experiments. Experimental results of the closed-loop displacement tracking have demonstrated that the delay time of the main valve is always within 3.5 ms under different working conditions, and the tracking error can be significantly reduced using the higher switching frequency. The amplitude–frequency experiments indicate that a −3 dB-frequency of the proposed valve can reach 9.5 Hz in the case of ±50% full scale and 15 Hz in the case of 0%–50% full scale. The values can be further improved by increasing the flow rate of the pilot HSV.

Keywords two-stage proportional valve, digital flow distribution, high-speed on/off valve, position tracking characteristic, dynamic performance

Received September 11, 2020; accepted November 25, 2020

Qiang GAO, Yuchuan ZHU (✉), Changwen WU, Yulei JIANG
National Key Laboratory of Science and Technology on Helicopter Transmission, Nanjing University of Aeronautics and Astronautics, Nanjing 210016, China
E-mail: meeyczhu@nuaa.edu.cn

1 Introduction

Electrohydraulic proportional systems are widely used in robots, aircraft actuators, tunnel boring machines, and wind power equipment owing to their good control accuracy and fast response [1,2]. Compared with the proportional valve system, a digital valve system (DVS) consisting of several on/off valves has certain advantages such as low throttling losses, good programmability, and high reliability. Nowadays, DVS is acquiescently considered a competitive alternative technology to the proportional system, as supported by research publications [3–5]. A high-speed on/off valve (HSV) serving as a core component in DVS works in a fully open or fully closed state. HSVs have also been widely used in electrohydraulic brake systems [6] and hydraulic pressure boost systems [7] owing to their several benefits, such as zero-structural dead band, high reliability, high efficiency, and low cost.

Many recent studies have focused on the structural optimization and controller optimization of HSVs. Paloniitty and Linjama [8] and Wu et al. [9] designed a miniature on/off valve by optimizing the distribution of the magnetic field. A self-correcting pulse width modulation (PWM) control proposed in Ref. [10] not only can improve the dynamic performance of the HSV but also maintain the same dynamic performance in different working conditions. Moreover, smart materials, such as piezoelectric [11], dielectric elastomer membrane [12], and giant magnetostrictive materials [13], are also applied to electromechanical converters of HSVs to improve dynamic performance, but this approach entails high cost and small output displacement.

However, increasing the HSV's output flow rate is more important in many high-power applications. The two conventional methods to achieve this objective are as follows: One is to improve the flow capacity of the HSV,

and the other is to design a parallel-connected DVS. As far as the HSV with large flow capacity is concerned, a two-stage structure is a common technique. Winkler et al. [14] proposed a new large flow switching valve, in which the pilot stage is a small fast switching valve and the main stage is a multi poppet valve. The nominal flow rate of the proposed valve is approximately 100 L/min. Wang et al. [15] designed a two-stage large-flow HSV for a hydraulic pressure converter, in which the three-way and two-position HSV of NACHI Company (Japan) was used in the pilot stage. As for the parallel-connected DVS, Matti Linjama and his research group [16] contributed numerous valuable works in this area. They first conducted a feasibility study on water–hydraulic parallel connection technology and experimentally verified that the parallel connection technology could effectively improve the efficiency of the system [16]. Some other new structures, such as the digital flow control unit [17] and the digital hydraulic power management system [18], were proposed for large flow applications in succession. Moreover, Lantela and Pietola [19] proposed a high-flow miniature DVS, in which the nominal flow of the P–A side is 30 L/min @ 0.5 MPa, and the laminated process technology was used for the valve manifold. The research results showed that the proposed DVS could control the flow instead of the standard proportional valve with ISO 03 [19].

In summary, the two conventional ways mentioned above can achieve a large flow rate, but problems still need to be overcome. For the HSV with a large flow capacity, as the high switching technology is used, the major challenges are the pressure fluctuation and vibration, especially in the high-pressure system. Moreover, the parallel-connected DVS needs a large number of on/off valves, which results in a comparatively large size and high cost of the valve package.

The priority control of the two-stage proportional control valve seems to be an effective way to obtain a large flow rate, in which the small flow rate HSV is used as the pilot stage and the large-sized spool is used as the main stage. The displacement of the main spool is approximately proportional to the duty cycle of the PWM signal. Compared with the two approaches mentioned above, the priority control has less vibration and can lessen the cost due to the use of small number of HSVs. A previous research [20] designed a novel configuration for a two-stage servo valve, in which two normally closed valves actuated by two piezoelectric ring benders were piloted to generate the control pressure. Zeng et al. [21] studied the influences of the pilot HSV's characteristics (voltage and duty cycle) on the performance of the main valve's displacement based on AMESim simulation. Wang et al. [22] studied the influences of certain factors (control signal, switching frequency, and pressure of the control chamber) on the dynamic performance of the main valve. Huang et al. [23,24] proposed a two-stage proportional flow control valve, in which the main stage was a flow amplifying valve and the pilot stage consisted of several on/off valves. In this study, the fluctuation of the pressure is analyzed by theoretical analysis, simulation, and testing. The research results indicate that a higher switching frequency of the HSV can smoothen pressure and displacement.

A novel two-stage proportional valve with a pilot digital flow distribution is proposed in this study. In Section 2, the working principle and mathematical model of the proposed valve are presented. In Section 3, the influences of the main parameters on the main valve's motion are analyzed. In Section 4, the value of the fixed orifice's diameter is optimized. In Section 5, the closed-loop displacement tracking and amplitude–frequency experiments are conducted. The main conclusions are summarized in Section 6.

2 Working principle and mathematical model

In this research, a two-stage proportional valve with a pilot digital flow distribution is proposed from the viewpoint of the dual nozzle-flapper's working principle, as shown in Fig. 1. In a traditional nozzle-flapper valve, the two variable orifices have a differential and coupled control. However, in this research, the dual nozzle-flapper is replaced by a digital flow distribution consisting of two HSVs, and the analog control signal is converted to digital.

The valve system consists of a pilot stage and the main stage with a linear variable differential transformer. The pilot stage consists of a digital flow distribution (HSV-A and HSV-B, i.e., two-position and two-way) and two fixed orifices, which are used to control the pressure and direction of the fluid flow in the pilot stage. The main stage is a pilot-operated spool valve, which is centered by a preload spring. In view of accurately controlling the output flow rate of the main valve, a position feedback control is established on the basis of the linear variable differential transformer and the control electronics.

The working principle can be described as follows:

1) In the inactive condition, the two HSVs are both de-energized. Additionally, the pressure in chamber A is the same as that in chamber B. Thus, the main valve maintains the central position by using the centering spring.

2) In the condition that the HSV-A is de-energized and the HSV-B is energized, the flow from chamber B to the tank (port T) through the HSV-B is provided. The pressure in chamber B decreases, causing the main valve to move to the right side.

3) In the condition that the HSV-A is energized and HSV-B is de-energized, the flow from chamber A to the tank (port T) through the HSV-A is provided. The pressure in chamber A decreases, causing that the main valve to move to the left side.

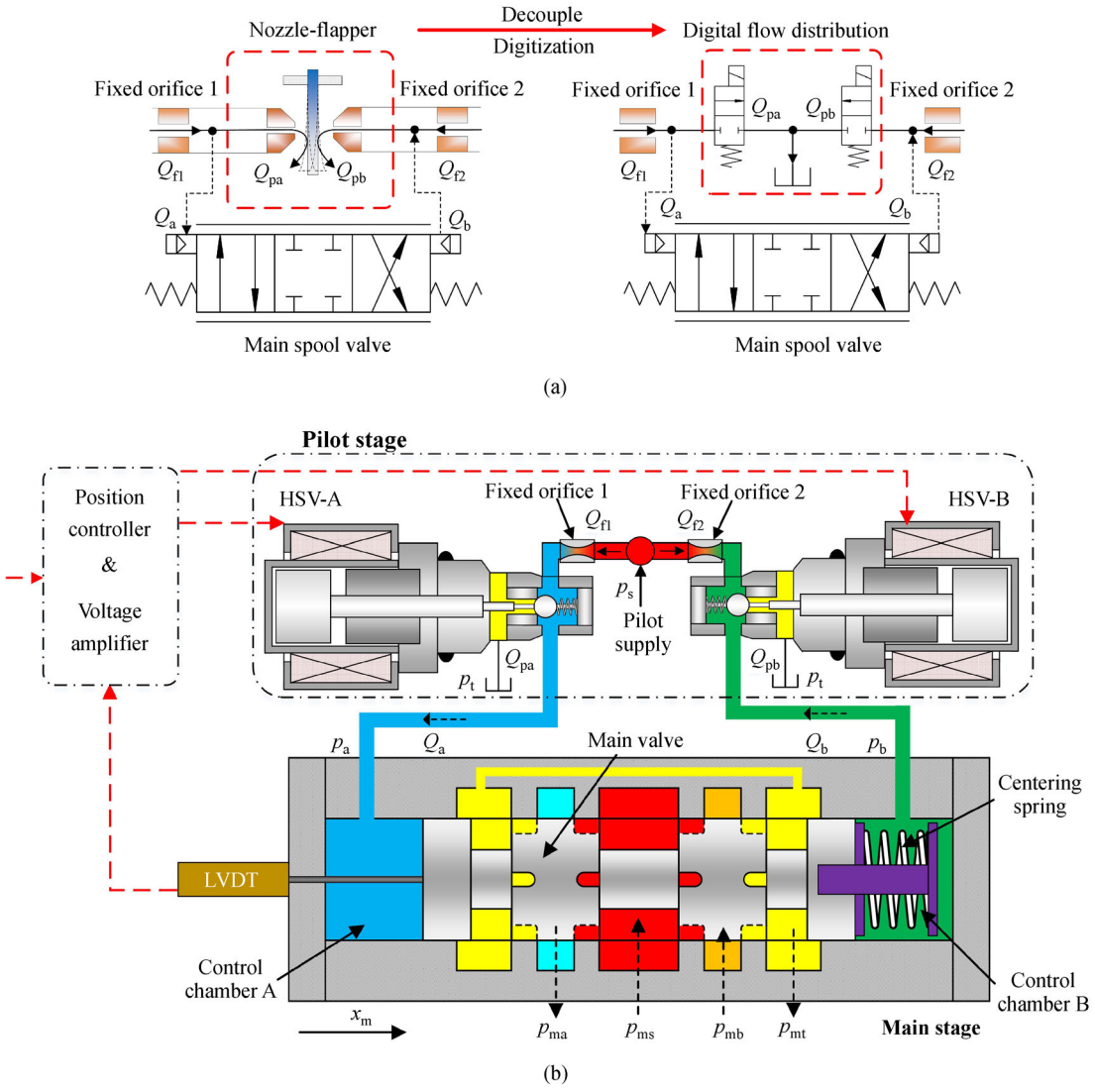

Fig. 1 Proposed two-stage proportional valve: (a) Schematic diagram and (b) structure diagram.

2.1 Model of the pilot stage

2.1.1 Dynamic characteristic of the pilot HSV

A two-position and two-way HSV is used in the pilot stage, as shown in Fig. 2. In actual scenarios, the motion of the ball valve lags behind the command PWM signal because of inductance and mechanical hysteresis. Therefore, the relationship between the HSV's opening area and the command PWM signal can be defined. As shown in Fig. 3,

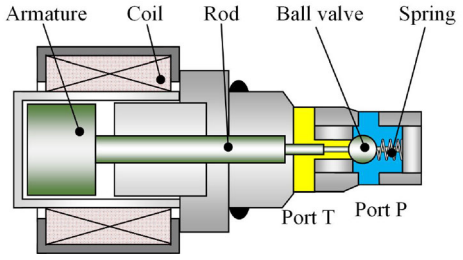

Fig. 2 Schematic diagram of the pilot high-speed on/off valve.

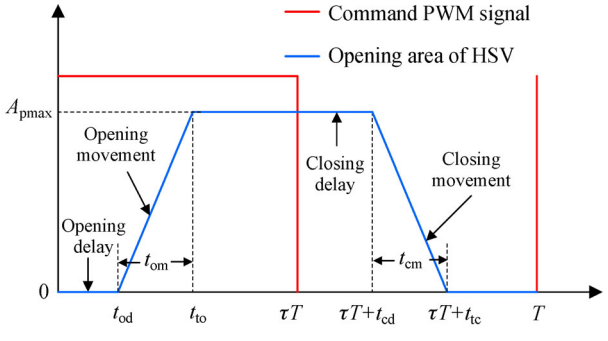

Fig. 3 Relationship between the HSV's opening area and the command PWM signal. HSV: High-speed on/off valve; PWM: Pulse width modulation.

t_{od} denotes the opening delay time; t_{om} denotes the opening movement time; t_{to} denotes the total opening time; t_{cd} denotes the closing delay time; t_{cm} denotes the closing movement time; t_{tc} denotes the total closing time; A_{pmax} denotes the maximum opening area of the pilot HSV; and T denotes the period of the PWM signal.

In the MATLAB/simulation platform, "transport delay module" and "rate limiter module" are used to regulate the opening/closing delay time and the opening/closing movement time, respectively. The dynamic model of the HSV is shown in Fig. 4.

2.1.2 Fluid model of the pilot stage

The modeling process of the proposed valve is similar to that of the traditional dual nozzle-flapper valve. As the two fixed orifices have the same structure, the flow rates of the two fixed orifices can be written as

$$Q_{f1} = C_f A_f \sqrt{\frac{2(p_s - p_a)}{\rho}}, \tag{1}$$

$$Q_{f2} = C_f A_f \sqrt{\frac{2(p_s - p_b)}{\rho}}, \tag{2}$$

where Q_{f1} and Q_{f2} denote the flow rates of the fixed orifices 1 and 2, respectively, p_s, p_a, and p_b denote the pilot supply pressure, the pressure in chamber A and chamber B, respectively, C_f and A_f denote the flow coefficient and the opening area of the fixed orifice, respectively, and ρ denotes the oil density.

The two HSVs with same structure are both controlled by the PWM signal. Thus, the output flow rate of the two HSVs are discrete in a single PWM period, which can be written as

$$Q_{pa} = \begin{cases} C_p A_{pmax} \sqrt{\dfrac{2(p_a - p_t)}{\rho}}, & 0 \leqslant t \leqslant \tau_1 T, \\ 0, & \tau_1 T < t \leqslant T, \end{cases} \tag{3}$$

$$Q_{pb} = \begin{cases} C_p A_{pmax} \sqrt{\dfrac{2(p_b - p_t)}{\rho}}, & 0 \leqslant t \leqslant \tau_2 T, \\ 0, & \tau_2 T < t \leqslant T, \end{cases} \tag{4}$$

where Q_{pa} and Q_{pb} denote the output flow rates of pilot HSV-A and pilot HSV-B, respectively, p_t denotes the pressure in the tank, C_p denotes the flow coefficient of the pilot HSV, and τ_1 and τ_2 denote the duty cycles of the PWM signal used for driving HSV-A and HSV-B, respectively.

In a single PWM signal period, the average output flow rates of the two HSVs can be also defined as [23]

$$\overline{Q}_{pa} = \tau_1 C_p A_{pmax} \sqrt{\frac{2(p_a - p_t)}{\rho}}, \tag{5}$$

$$\overline{Q}_{pb} = \tau_2 C_p A_{pmax} \sqrt{\frac{2(p_b - p_t)}{\rho}}, \tag{6}$$

where $\overline{Q}_{pa}$ and $\overline{Q}_{pb}$ denote the average output flow rates of HSV-A and HSV-B, respectively.

The net flow rates into chambers A and B (Q_a and Q_b) can be calculated by

$$\begin{aligned} Q_a &= Q_{f1} - \overline{Q}_{pa} \\ &= C_f A_f \sqrt{\frac{2(p_s - p_a)}{\rho}} - \tau_1 C_p A_{pmax} \sqrt{\frac{2(p_a - p_t)}{\rho}}, \end{aligned} \tag{7}$$

$$\begin{aligned} Q_b &= \overline{Q}_{pb} - Q_{f2} \\ &= \tau_2 C_p A_{pmax} \sqrt{\frac{2(p_b - p_t)}{\rho}} - C_f A_f \sqrt{\frac{2(p_s - p_b)}{\rho}}. \end{aligned} \tag{8}$$

The flow continuity equations of chambers A and B are written as

$$\frac{dp_a}{dt} = \frac{\beta}{V_{a0} + A_m x_m} \left(Q_a - A_m \frac{dx_m}{dt} - C_e p_a \right), \tag{9}$$

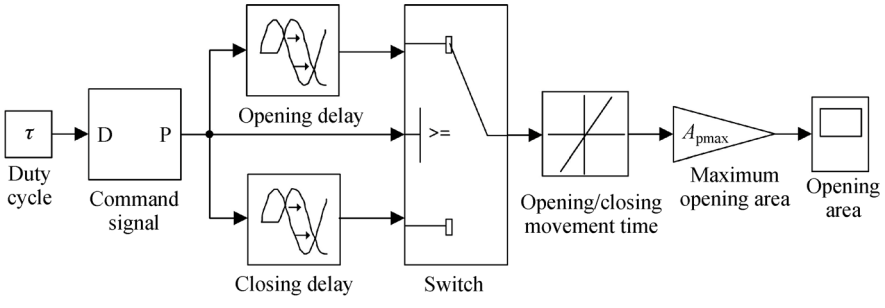

Fig. 4 Dynamic model of the pilot high-speed on/off valve.

$$\frac{\mathrm{d}p_\mathrm{b}}{\mathrm{d}t}=\frac{\beta}{V_{\mathrm{b}0}-A_\mathrm{m}x_\mathrm{m}}\left(A_\mathrm{m}\frac{\mathrm{d}x_\mathrm{m}}{\mathrm{d}t}-Q_\mathrm{b}-C_\mathrm{e}p_\mathrm{b}\right),\tag{10}$$

where $V_{\mathrm{a}0}$ and $V_{\mathrm{b}0}$ denote the initial volumes of chambers A and B, respectively, A_m denotes the cross-sectional area of the main valve, β denotes the fluid bulk modulus, C_e denotes the external leakage coefficient, and x_m denotes the displacement of the main valve.

2.2 Main valve stage

A three-position and four-way spool valve is selected as the main stage, as shown in Fig. 5.

By taking rightward motion of the main valve as an example, the force equilibrium equation of the main valve can be written as [25]

$$m_\mathrm{m}\ddot{x}_\mathrm{m}=(p_\mathrm{a}-p_\mathrm{b})A_\mathrm{m}-k_\mathrm{m}x_\mathrm{m}-F_\mathrm{mp}-B_\mathrm{m}\dot{x}_\mathrm{m}-F_\mathrm{mc}-F_\mathrm{ms},\tag{11}$$

where m_m denotes the equivalent mass of the main valve, B_m denotes the viscous friction coefficient of the main valve, k_m denotes the spring stiffness of the main valve, F_mp denotes the preload spring force of the main valve, F_mc denotes the Coulomb friction force of the main valve, and F_ms denotes the steady flow force of the main valve.

Assuming that the fluid velocity coefficient C_mv, the flow coefficient C_md, and fluid jet angle θ_m in the four variable orifices (P–A, P–B, A–T, and B–T) of the main valve are the same. Thus, the steady flow force F_ms of the main valve can be defined as

$$F_\mathrm{ms}=2C_\mathrm{mv}C_\mathrm{md}\cos\theta_\mathrm{m}\sum_{k=1}^{4}(A_k\Delta p_k),\tag{12}$$

where A_k denotes the opening area of the four variable orifices, and Δp_k denotes the pressure difference across the variable orifice.

In this case, the opening area of the main valve's variable orifices can be obtained by [26]

$$A_k=f(n,\ R_\mathrm{m},\ x_\mathrm{o})=\begin{cases}nR_\mathrm{m}^2\left[\arccos\left(1-\dfrac{x_\mathrm{o}}{R_\mathrm{m}}\right)-\left(1-\dfrac{x_\mathrm{o}}{R_\mathrm{m}}\right)\sqrt{\dfrac{x_\mathrm{o}}{R_\mathrm{m}}\left(2-\dfrac{x_\mathrm{o}}{R_\mathrm{m}}\right)}\right], & 0\leqslant x_\mathrm{o}\leqslant R_\mathrm{m},\\ \dfrac{\pi nR_\mathrm{m}^2}{2}+2nR_\mathrm{m}(x_\mathrm{o}-R_\mathrm{m}), & R_\mathrm{m}<x_\mathrm{o},\end{cases}\tag{13}$$

where n denotes the number of circular ports around the main valve, R_m denotes the radius of the circular ports around the main valve, and x_o denotes the opening of these circular ports.

The relationships between these orifice areas and the main valve's displacement are written as

$$A_\mathrm{pa}=\begin{cases}f(n_\mathrm{pa},\ R_\mathrm{m},\ x_\mathrm{m}-\Delta), & \Delta\leqslant x_\mathrm{m}\leqslant x_\mathrm{max},\\ 0, & x_\mathrm{m}<\Delta,\end{cases}\tag{14}$$

$$A_\mathrm{bT}=\begin{cases}f(n_\mathrm{bt},\ R_\mathrm{m},\ x_\mathrm{m}-\Delta), & \Delta\leqslant x_\mathrm{m}\leqslant x_\mathrm{max},\\ 0, & x_\mathrm{m}<\Delta,\end{cases}\tag{15}$$

$$A_\mathrm{pb}=\begin{cases}f(n_\mathrm{pb},\ R_\mathrm{m},\ -\Delta-x_\mathrm{m}), & -x_\mathrm{max}\leqslant x_\mathrm{m}\leqslant-\Delta,\\ 0, & x_\mathrm{m}>-\Delta,\end{cases}\tag{16}$$

$$A_\mathrm{aT}=\begin{cases}f(n_\mathrm{at},\ R_\mathrm{m},\ -\Delta-x_\mathrm{m}), & -x_\mathrm{max}\leqslant x_\mathrm{m}\leqslant-\Delta,\\ 0, & x_\mathrm{m}>-\Delta,\end{cases}\tag{17}$$

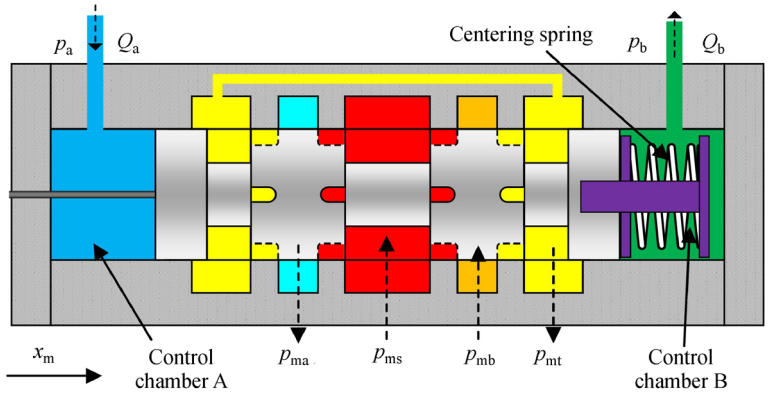

Fig. 5 Schematic diagram of the main valve.

where A_{pa} and A_{pb} denote the orifice areas from port P to ports A and B, respectively, A_{aT} and A_{bT} denote the orifice areas from port T to ports A and B, respectively, n_{pa} and n_{pb} denote the numbers of circular ports around the main valve's P–A port and P–B port ($n_{pa}=n_{pb}=2$), n_{at} and n_{bt} denote the numbers of circular ports around the main valve's A–T and B–T ports ($n_{at}=n_{bt}=4$), R_m denotes the radius of the circular ports, Δ denotes the center dead-band of the main valve (the left-center is the same as the right-center), and x_{max} denotes the maximum stroke.

The relationships between the displacement and these orifice areas, as determined by Eqs. (13)–(17), are shown in Fig. 6.

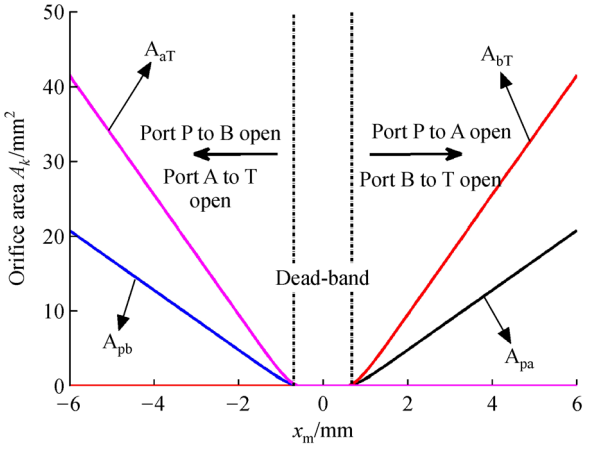

Fig. 6 Orifice area versus the main valve's displacement.

The main parameters used in this study are as follows [22,26–27]:

Opening delay time: $t_{od}=1.9$ ms;
Opening movement time: $t_{om}=1.1$ ms;
Closing delay time: $t_{cd}=2.6$ ms;
Closing movement time: $t_{cm}=2.6$ ms;
Maximum opening area of the HSV: $A_{pmax}=1.024$ mm^2;
Radius of the valve seat's hole: $r=0.66$ mm;
Flow coefficient of the HSV: $C_p=0.6$;
Flow coefficient of the fixed orifice: $C_f=0.85$;
Fluid jet angle: $\theta_m=69°$;
Radius of circular port: $R_m=1$ mm;
Cross-sectional area: $A_m=314$ mm^2;
Viscous friction coefficient: $B_m=17.6$ N/(m·s^{-1});
Coulomb friction force: $F_{mc}=8$ N;
Initial volume of chamber A: $V_{a0}=3750$ mm^3;
Initial volume of chamber B: $V_{b0}=3750$ mm^3;
Center dead-band: $\Delta=0.62$ mm;
Main stage spring preload: $F_{mp}=50$ N;
Mass of the main valve: $m_m=205$ g;
Main stage spring stiffness: $k_m=50$ N/mm;
Flow coefficient of the main valve: $C_{md}=0.61$;
Fluid velocity coefficient of the main valve: $C_{mv}=0.98$.

3 Relationship between the main valve's motion and main parameters

3.1 Analysis of the main valve's motion

The characteristic of the main valve's motion is analyzed on the basis of the relationship between the PWM signal and the main valve's displacement, as shown in Fig. 7, in which the rightward motion is taken as an example. In Fig. 7, Δx_1 denotes the displacement of the main valve moving to the right in a single period; Δx_2 denotes the displacement of the main valve moving to the left in a single period; and Δx_e denotes the effective displacement of the main valve moving to the right in a single period.

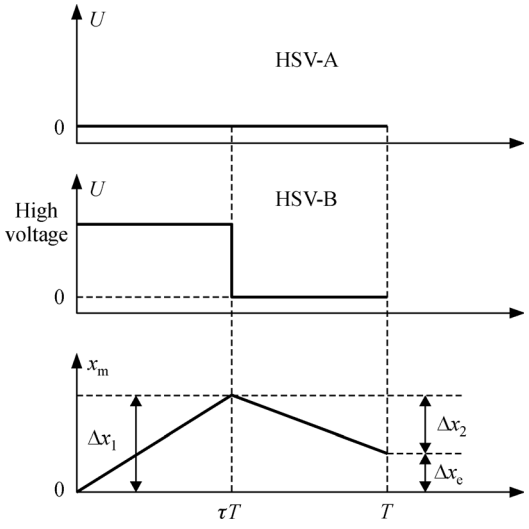

Fig. 7 Relation between the PWM signal and the main valve's motion.

Similarly, as shown in Fig. 7, the main valve moves to the right due to the pressure difference in the two chambers during the high-voltage period ($0<t<\tau T$). By contrast, during the zero-voltage period ($\tau T<t<T$), the main valve moves to the left due to the spring force. In addition, when Δx_1 and Δx_2 simultaneously increase, the fluctuation of the main valve's motion increases. The ideal condition is for Δx_1 to be much larger and Δx_2 to be much smaller, and they are obtained simultaneously. In this manner, a larger effective displacement and a smaller displacement fluctuation can be achieved.

For the high-voltage period ($0<t<\tau T$), Eqs. (9) and (10) can be rewritten as

$$\Delta p_{a1}=\frac{\beta}{V_{a0}+A_m x_m}\left(Q_{a1}-A_m\frac{dx_m}{dt}-C_t p_a\right)\Delta t, \quad (18)$$

$$\Delta p_{b1}=\frac{\beta}{V_{b0}-A_m x_m}\left(A_m\frac{dx_m}{dt}-Q_{b1}-C_t p_b\right)\Delta t, \quad (19)$$

where Δp_{a1} and Δp_{b1} denote the pressure fluctuations in chambers A and B during the period $(0<t<\tau T)$, respectively, while Q_{a1} and Q_{b1} denote the net flow rates into chambers A and B during the period $(0<t<\tau T)$, respectively.

Assume that the initial volume of the chamber is much greater than the change in volume caused by the movement of the main valve, and the external leakage is ignored [23]. Equations (18) and (19) can be rewritten as

$$\Delta p_{a1}=\frac{\beta\Delta t}{V_{a0}}Q_{a1}=\frac{\beta\tau}{V_{a0}f}Q_{a1}, \tag{20}$$

$$\Delta p_{b1}=-\frac{\beta\tau}{V_{b0}f}Q_{b1}, \tag{21}$$

where f denotes the carrier frequency of the PWM signal.

The net flow rate into chambers A and B (Q_{a1} and Q_{b1}) during the period $(0<t<\tau T)$ are as follows:

$$Q_{a1}=C_fA_f\sqrt{\frac{2(p_s-p_a)}{\rho}}, \tag{22}$$

$$Q_{b1}=C_pA_{pmax}\sqrt{\frac{2(p_b-p_t)}{\rho}}-C_fA_f\sqrt{\frac{2(p_s-p_b)}{\rho}}. \tag{23}$$

Then, the value of Δx_1 can be calculated by

$$\begin{aligned}\Delta x_1&=\frac{|\Delta p_{a1}-\Delta p_{b1}|A_m}{k_m}=\frac{\beta\tau A_m}{V_{a0}fk_m}(Q_{a1}+Q_{b1})\\&=\frac{\beta\tau A_m}{V_{a0}fk_m}\sqrt{\frac{2}{\rho}}[C_pA_{pmax}\sqrt{p_b}\\&\quad+C_fA_f(\sqrt{p_s-p_a}-\sqrt{p_s-p_b})].\end{aligned} \tag{24}$$

Conversely, during the zero-voltage period $(\tau T<t<T)$ when HSV-A is de-energized and HSV-B is driven by zero voltage, the models of control chambers A and B can be defined as

$$\Delta p_{a2}=-\frac{\beta\Delta t}{V_{a0}}Q_{a2}=-\frac{\beta(1-\tau)}{V_{a0}f}Q_{a2}, \tag{25}$$

$$\Delta p_{b2}=\frac{\beta\Delta t}{V_{b0}}Q_{b2}=\frac{\beta(1-\tau)}{V_{b0}f}Q_{b2}, \tag{26}$$

where Δp_{a2} and Δp_{b2} denote the pressure fluctuations in chambers A and B during the period $(\tau T<t<T)$, respectively, and Q_{a2} and Q_{b2} denote the net flow rates into chambers A and B during the period $(\tau T<t<T)$, respectively.

Q_{a2} and Q_{b2} are expressed as

$$Q_{a2}=C_fA_f\sqrt{\frac{2(p_s-p_a)}{\rho}}, \tag{27}$$

$$Q_{b2}=C_fA_f\sqrt{\frac{2(p_s-p_b)}{\rho}}. \tag{28}$$

Assuming that the acceleration of the main valve remains the same during the period $(\tau T<t<T)$, the value of Δx_2 can be calculated by

$$\begin{aligned}a_m&=\frac{F_m(\Delta x_1)-|\Delta p_{b2}+\Delta p_{a2}|A_m}{m_m}\\&=\frac{F_m(\Delta x_1)}{m_m}-\frac{\beta(1-\tau)A_m|Q_{b2}-Q_{a2}|}{V_{a0}fm_m},\end{aligned} \tag{29}$$

$$\begin{aligned}\Delta x_2&=\frac{1}{2}a_m\Delta t^2=\frac{(1-\tau)^2F_m(\Delta x_1)}{2m_mf^2}\\&\quad+\frac{\beta(1-\tau)^3A_m}{2V_{a0}m_mf^3}|Q_{b2}-Q_{a2}|=\frac{(1-\tau)^2F_m(\Delta x_1)}{2m_mf^2}\\&\quad+\frac{\beta(1-\tau)^3A_m}{2V_{a0}m_mf^3}C_fA_f\sqrt{\frac{2}{\rho}}|\sqrt{p_s-p_b}-\sqrt{p_s-p_a}|,\end{aligned} \tag{30}$$

where a_m and $F_m(\Delta x_1)$ denote the acceleration and spring force of the main valve when the main valve's displacement equals to Δx_1.

Therefore, the effective displacement of the main valve Δx_e is

$$\Delta x_e=\Delta x_1-\Delta x_2. \tag{31}$$

The relationships between the parameters and the main valve's displacement are obtained on the basis of Eqs. (24), (30), and (31), as shown in Table 1.

Table 1 Relationships between parameters and displacement

Parameter	Δx_1	Δx_2	Δx_e	Displacement fluctuation
$\tau\uparrow$	↑	↓	↑	↓
$f\uparrow$	↓	↓	↓	↓
$k_m\downarrow$	↑	↓	↑	↓
$A_f=\pi d_f^2/4\uparrow$	↑	↑	↑ & ↓	↑

Table 1 clearly shows that the duty cycle τ increases, resulting in the increase of the Δx_e and the reduction of the displacement fluctuation. The switching frequency f increases, leading to in the reduction of the Δx_e and the displacement fluctuation. The spring stiffness k_m decreases, resulting in the increase of the Δx_e and the reduction of displacement fluctuation. However, the influence of the fixed orifice's diameter d_f on the Δx_e becomes complex and thus needs to be studied and optimized, as to be discussed in the next section.

3.2 Simulation results of the parameters' influences

Section 3.1 simply qualitatively analyzes the relationship between the parameters and motion of the main valve. The mathematical model established in Section 2, which is simulated using MATLAB/Simulink, can quantitatively analyze the influences of the parameters (k_m, τ, f, and d_f) on the displacement of the main valve (Fig. 8).

The influences of spring stiffness k_m on the motion of the main valve are shown in Fig. 8(a). In Fig. 8(a), τ, f, and d_f are set as 0.5, 50 Hz, and 0.5 mm, respectively. With the increase in k_m, the main valve's effective displacement decreases and the main valve's displacement fluctuation increases due to the relatively large motion resistance (spring force). In addition, the larger is the main valve's displacement, the larger is the spring force, which leads to a larger return displacement (Δx_2). This issue causes a significant fluctuation in the main valve's displacement. Therefore, a much smaller spring stiffness k_m is beneficial for improving the effective displacement and reducing the displacement fluctuation.

The influences of duty cycle τ on the main valve's motion, are shown in Fig. 8(b). In the figure, k_m, f, and d_f are set as 50 N/mm, 50 Hz, and 0.5 mm, respectively. With the increase in τ, the Δx_1 increases whereas Δx_2 decreases due to the relatively long excitation time of the high voltage. Thus, a much larger value of τ is beneficial for improving the effective displacement Δx_e and reducing the displacement fluctuation.

The influences of switching frequency f on the main valve's motion are shown in Fig. 8(c). In Fig. 8(c), k_m, τ, and d_f are set as 50 N/mm, 0.5, and 0.5 mm, respectively. As f increases, the time required for a single-PWM signal period decreases, which is beneficial for improving the output flow resolution. As a means of obtaining the same displacement, more switching numbers are used when using the higher frequency, which leads to a smaller displacement error. In addition, the fluctuation of the main valve's displacement is smaller under the higher switching frequency.

The influences of the fixed orifice diameter d_f on the main valve's motion are shown in Fig. 8(d). In Fig. 8(d), k_m, τ, and f are set as 50 N/mm, 0.5, and 50 Hz, respectively. With the increase in d_f, the Δx_1 and Δx_2 both increase due to the larger flow rate into the two control chambers of the main valve, but the change in Δx_2 is more obvious. In addition, the larger is the value of d_f, the larger is the fluctuation of the main valve's displacement. Thus, d_f has complex effects on the main valve's motion, which needs to be optimized.

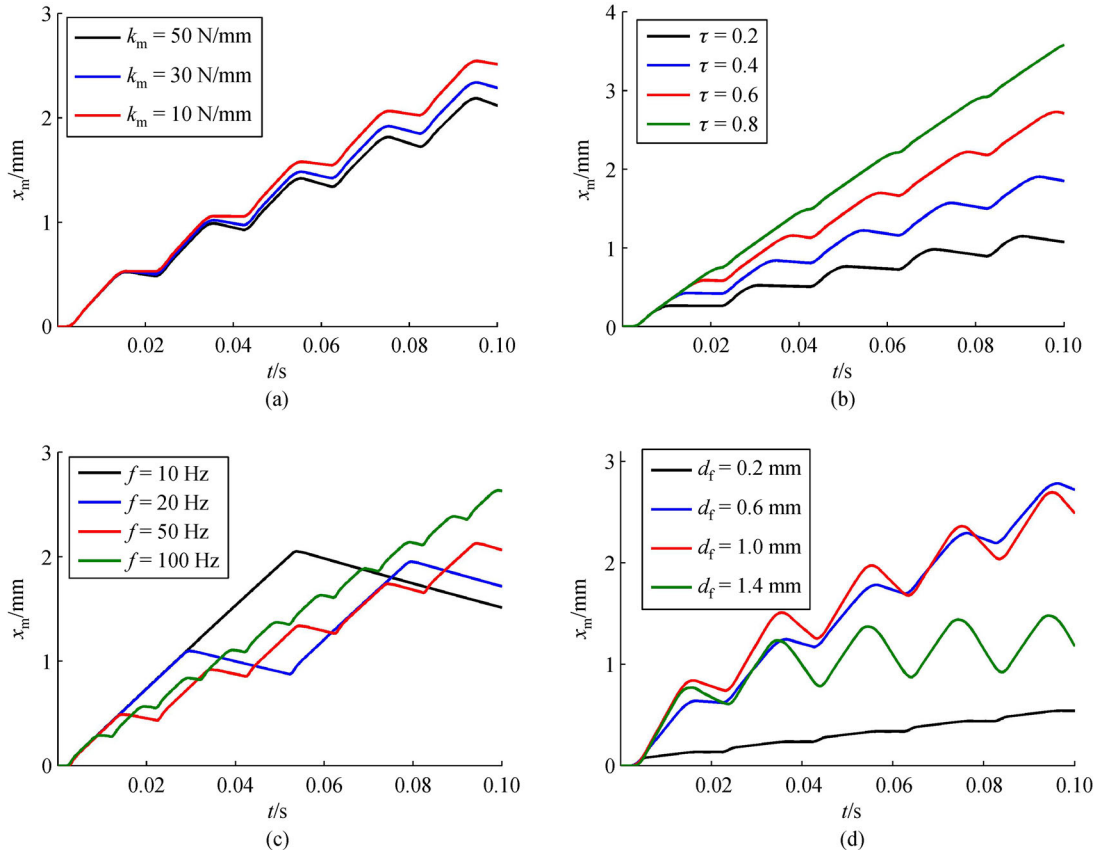

Fig. 8 Influences of the parameters on the displacement of the main valve. Influence of (a) spring stiffness k_m, (b) duty cycle τ, (c) switching frequency f, and (d) fixed orifice diameter d_f on the main valve's motion.

4 Optimization of the fixed orifice's diameter (d_f)

4.1 Design criterion of d_f

The working principle of the proposed pilot stage is the same as that of the dual nozzle-flapper, as shown in Fig. 9. The two fixed orifices are used to produce control pressures p_a and p_b, which can be modulated by regulating the duty cycles of the PWM signals. The hole of the valve seat is equivalent to that of the nozzle. The initial duty cycle τ_0 in the proposed stage is equivalent to the flapper's null position in the traditional dual nozzle-flapper valve. As the HSV used in this study is a commercial valve, a design criterion of the fixed orifice's diameter based on the maximum control pressure sensitivity is proposed under the premise that the structural parameters of the HSV are known.

The flow equations are written as follows to be able to analyze the control pressure sensitivity:

$$\begin{aligned} Q_a &= Q_{f1} - \overline{Q}_{pa} \\ &= C_f A_f \sqrt{\frac{2(p_s - p_a)}{\rho}} - C_p A_{pmax}(\tau_0 - \tau)\sqrt{\frac{2p_a}{\rho}}, \end{aligned} \tag{32}$$

$$\begin{aligned} Q_b &= \overline{Q}_{pb} - Q_{f2} \\ &= C_p A_{pmax}(\tau_0 + \tau)\sqrt{\frac{2p_b}{\rho}} - C_f A_f \sqrt{\frac{2(p_s - p_b)}{\rho}}, \end{aligned} \tag{33}$$

where τ_0 and τ are the initial duty cycle and the control duty cycle, respectively.

If there is no flow to the main valve, that is, the load is blocked, then $Q_a = Q_b = 0$, which results in the following simplified equation:

$$\frac{p_a}{p_s} = \left[1 + \left(\frac{C_p A_{pmax}(\tau_0 - \tau)}{C_f A_f}\right)^2\right]^{-1}. \tag{34}$$

The behavior described by Eq. (34) for the blocked characteristics is plotted in Fig. 10.

Let

$$a = \frac{C_p A_{pmax}\tau_0}{C_f A_f}, \tag{35}$$

then,

$$\frac{p_a}{p_s} = \left[1 + a^2\left(1 - \frac{\tau}{\tau_0}\right)^2\right]^{-1}. \tag{36}$$

The pressure sensitivity at the null point is given by

$$\left.\frac{dp_a}{d\tau}\right|_{\tau=0} = \frac{p_s}{\tau_0}\frac{2a^2}{(1+a^2)^2}. \tag{37}$$

The maximum pressure sensitivity can be achieved if the following equation is satisfied:

$$\frac{d}{da}\left(\left.\frac{dp_a}{d\tau}\right|_{\tau=0}\right) = \frac{p_s}{\tau_0}\frac{4a(1-a^2)}{(1+a^2)^3}. \tag{38}$$

Thus, if

$$a = \frac{C_d A_{pa}\tau_0}{C_f A_f} = \frac{C_p A_{pmax}\tau_0}{C_f \pi d_f^2/4} = 1, \tag{39}$$

then the maximum pressure sensitivity can be obtained.

The value of the fixed orifice's diameter d_f is written as

$$d_f = \sqrt{\frac{4C_p A_{pmax}\tau_0}{C_f \pi}}. \tag{40}$$

According to Eq. (40), the initial duty cycle τ_0 is the key element for calculating the d_f. In obtaining the initial duty

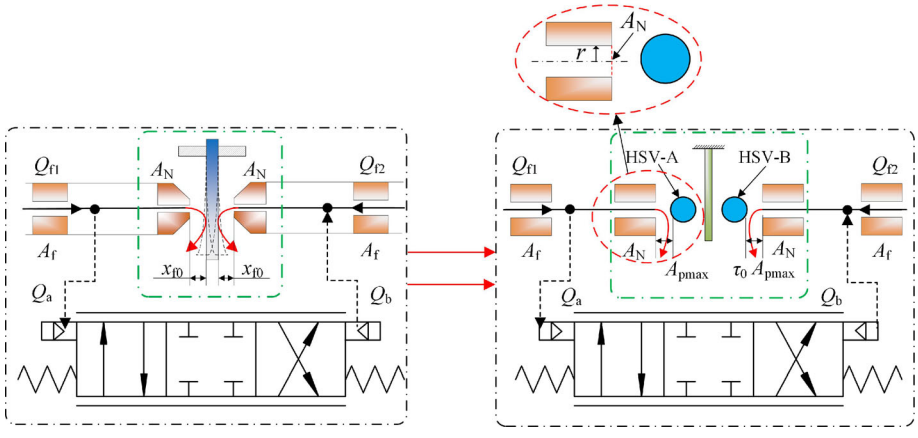

Fig. 9 Relation between the dual nozzle-flapper valve and proposed valve.

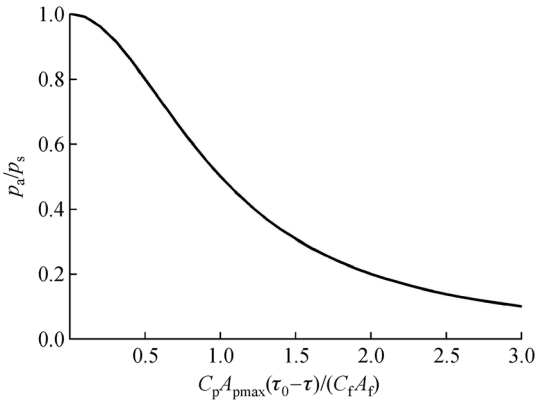

Fig. 10 Blocked load characteristics.

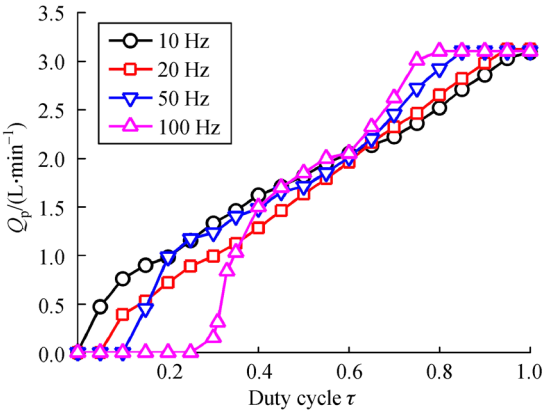

Fig. 11 Flow characteristics of the high-high-speed on/off valve.

cycle τ_0, a design criterion based on flow controllability and flow linearization is proposed. The flow controllability principle of the traditional dual nozzle-flapper is also applicable to the pilot stage of this study, in which the opening area of pilot HSV is smaller than that of the nozzle to avoid flow saturation. Therefore, the following equation is often given [27]:

$$A_{pmax}\tau_0 \leqslant \frac{1}{4}A_N = \frac{1}{4}\pi r^2, \tag{41}$$

where A_N and r denote the area (flow area of the valve seat's hole) and radius (radius of the valve seat's hole) of the nozzle, respectively.

According to Eq. (41), good flow controllability can be obtained if the following equation is satisfied:

$$\tau_0 \leqslant 0.334. \tag{42}$$

However, the linearity of the pilot HSV's output flow is an important issue requiring simultaneous attention. When the HSV is driven by the PWM signal, the static flow of the HSV indeed has a dead band (in small duty cycle) and saturation (in larger duty cycle), which may worsen the tracking performance of the main valve as a result of electrical and mechanical lag, as shown in Fig. 11.

As shown in Fig. 11, when the duty cycle is in the range of 0.45–0.95 at 10 Hz, 0.15–0.9 at 20 Hz, 0.5–0.8 at 50 Hz, and 0.4–0.6 at 100 Hz, the linearity of the HSV output flow is satisfactory. Therefore, in achieving a balance between the flow controllability and flow linearity of the pilot HSV, the initial duty cycle τ_0 is selected as 0.5.

Subsequently, Eq. (40) can be rewritten as

$$d_f = \sqrt{\frac{2C_pA_{pmax}}{C_f\pi}} = 0.68. \tag{43}$$

4.2 Simulation result of the designed d_f

Simulations are performed to verify the effectiveness of the proposed d_f, as shown in Fig. 12.

As shown in Fig. 12, with the designed d_f, the balance between the effective displacement and the displacement fluctuation of the main valve can be enhanced. A large effective displacement can be achieved with small fluctuation.

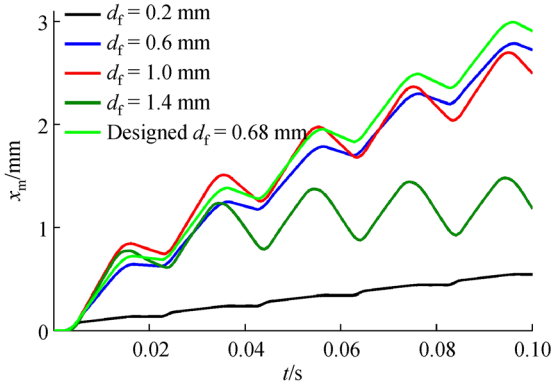

Fig. 12 Influences of the designed d_f on the displacement of the main valve.

5 Experimental results

In studying the performance of the proposed two-stage proportional valve, comprehensive performance tests are conducted on a hydraulic test platform. The set-up is shown in Fig. 13.

The platform mainly consists of a two-stage proportional valve with a designed digital flow-distribution pilot stage, an xPC real-time controller, and a hydraulic power supply. The xPC real-time controller is composed of a master and slave computer and a data acquisition and control card (NI PCI 6251). The PWM signals proposed in Ref. [28] are designed in MATLAB/Simulink to drive the HSV. Furthermore, the data for control pressure and position are collected and transferred to the PCI 6251 through the differential transfer module. The HSV drive card is used to

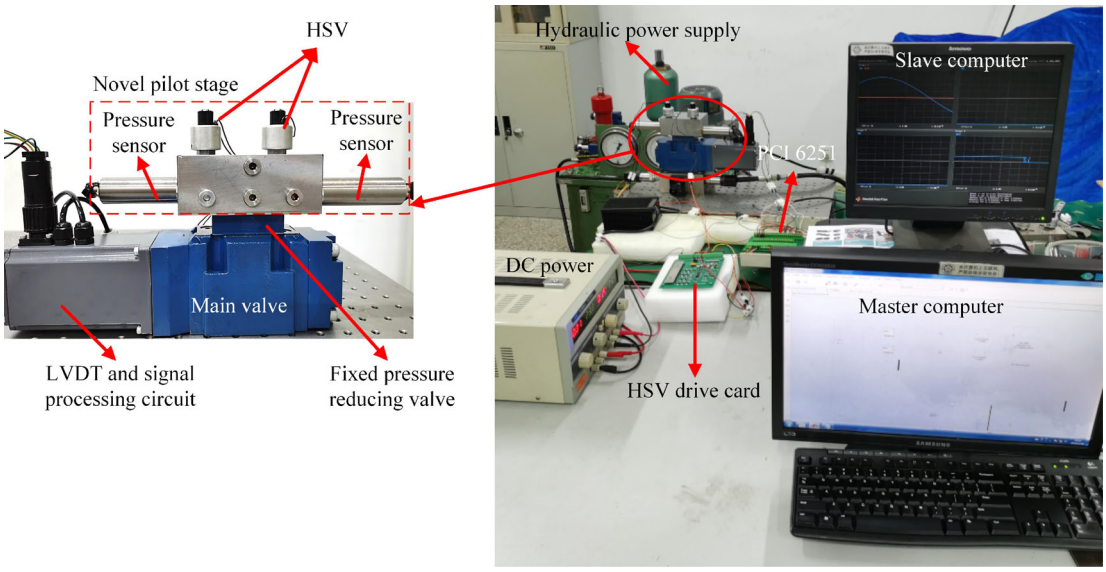

Fig. 13 Performance test bench of the proposed two-stage proportional valve.

amplify the 5 V PWM signal output by PCI 6251 into a 24 V PWM signal for driving the HSVs. Two high-frequency pressure sensors (Kunshan Shuanqiao CYG1401F; accuracy of 0.5%, response frequency of 20 kHz) are used to measure control pressure of chambers A and B. The closed-loop controller of the main valve's displacement is implemented in by MATLAB/Simulink, which needs to be compiled into the discretization C++ codes.

The main valve stage is taken from the same part of the commercial pilot proportional valve (4WRKE10E100, Jiangsu Hengli Hydraulic Co., Ltd., China). The rated pressure and rated flow rate of the main valve stage can reach 31.5 MPa and 100 L/min, respectively. However, the rated pressure and rated flow rate of the designed pilot valve stage are 10 MPa and 6 L/min. As the rated pressure and rated flow rate of the pump station are only 8 MPa and 10 L/min, the hydraulic supply pressure is set as 7 MPa in the experiments and simulations. Then, the proposed valve is compared with the existing commercial valve under the same working conditions. The compared result is fair and credible. In future studies, we will focus on the performance of the proposed valve under high-pressure and large flow rate conditions.

5.1 Influences of the main parameters

The influences of duty cycle τ on the main valve's displacement are shown in Fig. 14(a). In Fig. 14(a), f and d_f are set as 50 Hz and 0.5 mm, respectively. The test results are the same as the simulation results previously illustrated in Fig. 8(b). The effective displacement Δx_e of the main valve increases because the much larger τ, leading to a longer high-voltage excitation time of HSV-B's PWM signal.

The influences of the switching frequency f on the main valve's displacement are shown in Fig. 14(b). In Fig. 14(b), τ and d_f are set as 0.5 and 0.5 mm, respectively. The test results are also the same as the simulation results previously shown in Fig. 8(c). With the increase in switching frequency f, more switching numbers of HSV-B can be observed in the same time range, leading to a smaller fluctuation of the main valve's displacement. As such, the improvement of f is beneficial for reducing the tracking error of the main valve's displacement.

The influences of the fixed orifice diameter d_f on the main valve's displacement are shown in Fig. 14(c). In the figure, τ and f are set as 0.5 and 50 Hz, respectively. The experimental results indicate that the optimized value of the fixed orifice diameter d_f is 0.6 mm, which is slightly smaller than the simulation result of 0.68 mm previously shown Fig. 8(d). This finding can be attributed to the fixed orifice installed onto the pilot valve body through the thread, and the thread gap generates an annular leakage under the pressure difference. In addition, considering the difficulty of manufacturing small-diameter fixed orifices, the fixed orifice with a diameter of 0.6 mm is selected as the final optimization result.

5.2 Performance of step response

The experimental results of the step response of the main valve are shown in Fig. 15. The reference step signal is 3 mm, and the switching frequencies are selected as 50 and 100 Hz. As shown in Fig. 15, the delay times under different switching frequencies are small (only 3.5 ms) which only relates to the opening time of the HSV. In addition, with the increase in the switching frequency, the steady displacement error decreases due to the higher resolution of the HSV's output flow rate. For example,

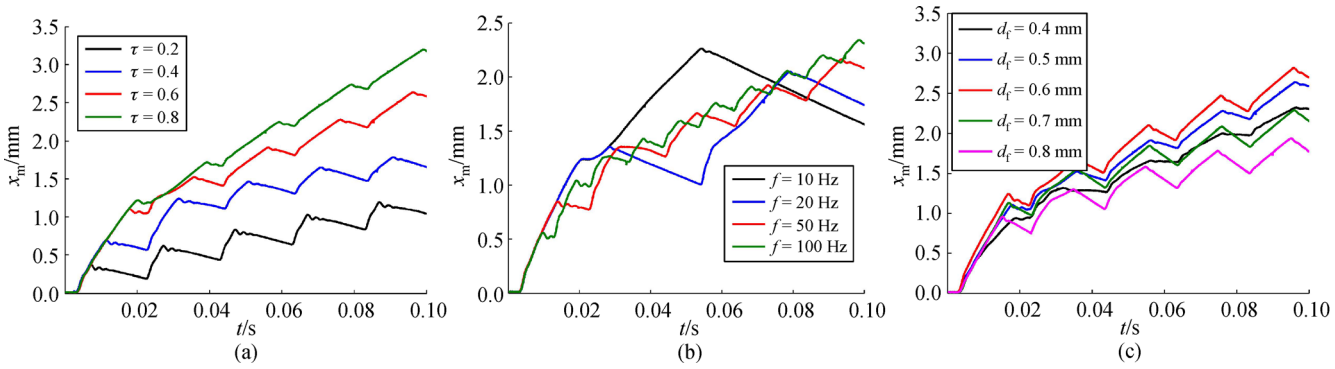

Fig. 14 Influences of (a) duty cycle τ, (b) switching frequency f, and (c) fixed orifice diameter d_f on the main valve's displacement.

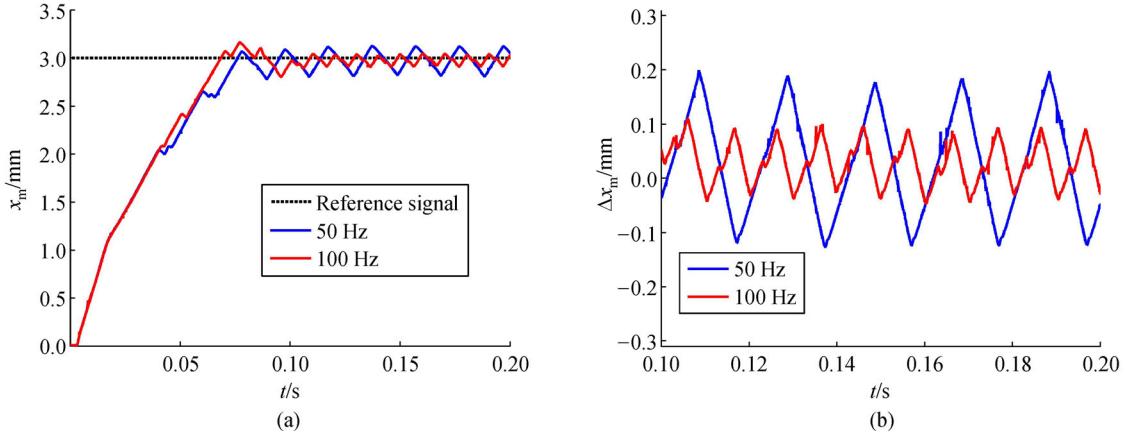

Fig. 15 Step responses of the main valve's displacement under different switching frequencies: (a) Tracking displacement and (b) steady tracking error.

compared with the switching frequency of 50 Hz, the maximum steady displacement error is reduced by 45% (0.11 mm) when using the switching frequency of 100 Hz.

5.3 Performance of sinusoidal tracking

Sinusoidal tracking performance of the main valve's displacement under different switching frequencies are shown in Fig. 16. For the proposed valve with the PID closed-loop controller, the sinusoidal tracking can be achieved. Additionally, the larger the reference displacement frequency, the larger the lag time which is limited by the flow rate of the pilot HSV.

In assessing the performance of the sinusoidal tracking, the maximum tracking error M_e, average tracking error μ, and standard deviation of the tracking error σ in publication [29] are used. A comparison of the sinusoidal tracking errors under different switching frequencies is shown in Table 2.

The comparative results shown in Table 2 clearly indicate that, with respect to the switching frequency of 50 Hz, the tracking error is significantly reduced when 100 Hz is used. The trend is due to the much higher resolution of the output flow rate. In addition, due to the fixed control parameters used for the PID controller, there is no guarantee that optimal control can be achieved under different working conditions. The advanced control strategies for this valve will be investigated in a future study.

5.4 Amplitude–frequency characteristic

Comparison of the amplitude–frequency characteristics between the proposed valve and the existing valve is shown in Fig. 17. A –3 dB-frequency of the proposed proportional valve can reach 9.5 Hz in the case of ±50% full scale and 15 Hz in the case of 0%–50% full scale. In addition, the amplitude–frequency of the proposed valve is smaller than that of the existing commercial valve because the pilot HSV's flow is smaller than that of the existing pilot proportional valve. We will focus on the flow improvement of the pilot HSV in the future as a means of improving the amplitude–frequency of the proposed valve.

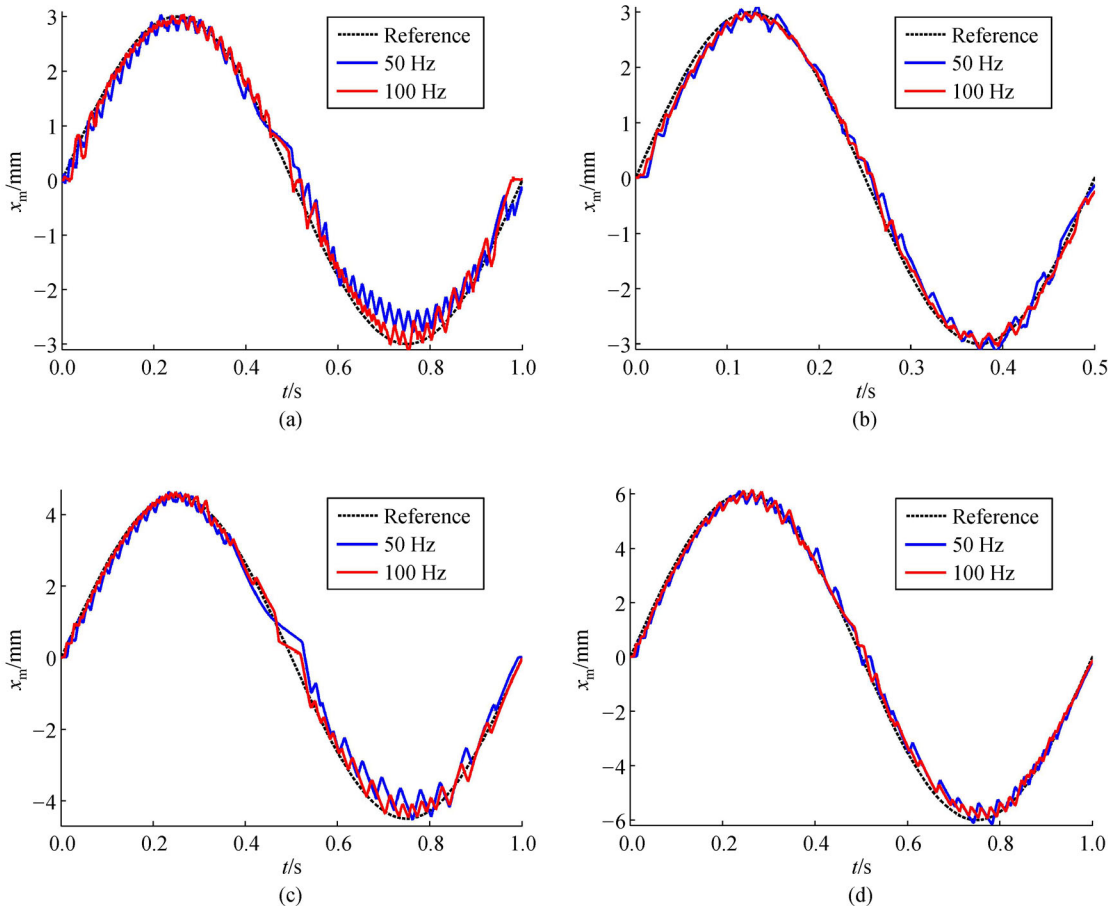

Fig. 16 Sinusoidal tracking of the main valve's displacement under different switching frequencies: (a) Amplitude is 3 mm and frequency is 1 Hz, (b) amplitude is 3 mm and frequency is 2 Hz, (c) amplitude is 4.5 mm and frequency is 1 Hz, and (d) amplitude is 6 mm and frequency is 1 Hz.

Table 2 Comparison of sinusoidal tracking errors under different switching frequencies

Sinusoid tracking	Switching frequency/Hz	M_e/mm	μ/mm	σ/mm
Signal 1 (amplitude is 3 mm and frequency is 1 Hz)	50	0.682	0.218	0.270
	100	0.531	0.143	0.109
Signal 2 (amplitude is 3 mm and frequency is 2 Hz)	50	0.449	0.145	0.176
	100	0.343	0.112	0.139
Signal 3 (amplitude is 4.5 mm and frequency is 1 Hz)	50	1.081	0.292	0.362
	100	0.644	0.150	0.197
Signal 4 (amplitude is 6 mm and frequency is 1 Hz)	50	0.765	0.225	0.277
	100	0.579	0.179	0.219

6 Discussion

The comparisons between the simulations and experiments of the main valve's displacement under different duty cycles and variations in the fixed orifice's diameters are shown in Fig. 18.

As shown in Fig. 18, the changing rules of the simulations are the same as those of the experiments under different duty cycles and fixed orifice's diameters. However, the results of the simulations and experiments somewhat differ. This finding may have been caused by certain factors, such as the unmodeled transient flow force of the main valve and the varying flow coefficient. In this study, the flow coefficient of the pilot HSV is taken from Ref. [22] and finely tuned to meet the maximum flow rate. In addition, the flow coefficients of the fixed orifice and the

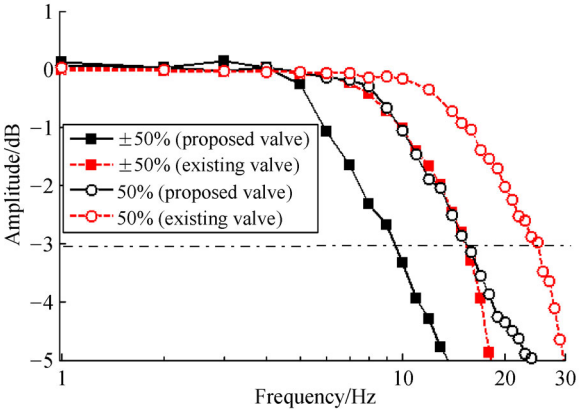

Fig. 17 Comparison of the amplitude–frequency characteristics between the proposed valve and the existing valve.

main valve are set with constant values (0.85 and 0.61), as adopted from Ref. [27].

However, the flow coefficient of the valve is related to the valve's opening and the pressure difference across the valve. For example, the flow coefficient is low at the small valve's opening and high at the large valve's opening, which have already been verified in Refs. [30,31]. The innovations of this research are to develop a novel two-stage proportional valve and present a new design criterion. In the future, we will focus on how to accurately predict the flow coefficient through flow-field simulation as a means of improving the accuracy of the simulation model.

7 Conclusions

In this study, a novel two-stage proportional valve with a pilot digital flow distribution is proposed from the special viewpoint of the dual nozzle-flapper's working principle. The working principle and mathematical model of the proposed valve are determined. Extensive simulations and experiments have been conducted to analyze the performances of the proposed valve.

The main conclusions are as follows:

1) The influences of the control parameters (duty cycle τ and switching frequency f) and the structural parameters (fixed orifice's diameter d_f and main valve's spring k_m) on the main valve's movement characteristic are analyzed by theory, simulation, and experiment. The results indicate that a much larger τ is beneficial for improving the effective displacement. The large f and the small k_m are used to reduce the displacement fluctuation. Moreover, d_f has complex effects on the main valve' movement characteristic.

2) In optimizing the value of d_f, a new design criterion that considers the maximum pressure sensitivity, flow controllability, and flow linearization is proposed to improve the balance between the effective displacement and the displacement fluctuation of the main valve. The results have been verified by simulations and experiments.

3) The experimental results of the step response indicate that the delay times are only within 3.5 ms under different working conditions, and the maximum steady error significantly decreases with the increase in switching frequency. Moreover, the results of the sinusoid displacement tracking demonstrate that a much smaller tracking error can be achieved using a much higher switching frequency.

4) The amplitude–frequency experiments indicate that a –3 dB-frequency of the proposed valve can reach 9.5 Hz in the case of ±50% full scale and 15 Hz in the case of 0%–50% full scale.

In the future, our work shall focus on the flow improvement of the pilot valve and the optimization of control strategies to improve the performance of the proposed valve.

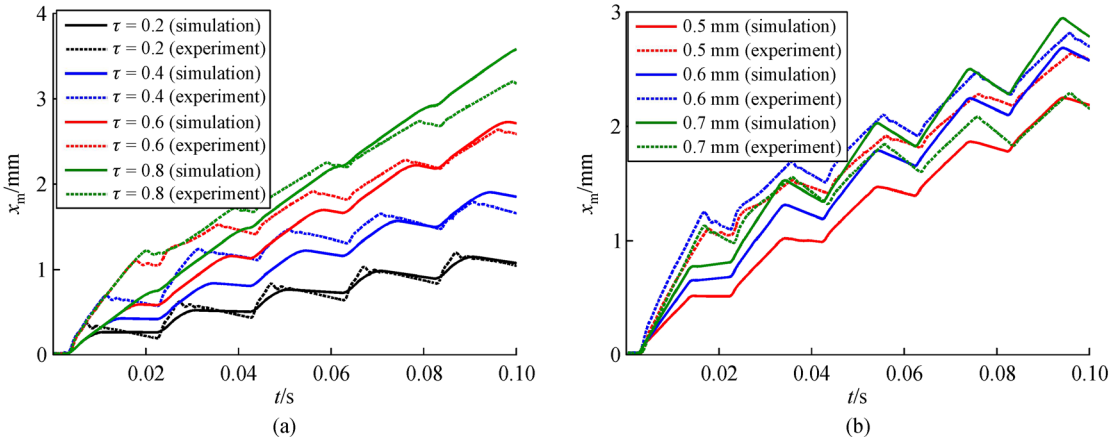

Fig. 18 Comparisons between simulations and experiments of the main valve's displacement: Under different (a) duty cycles and (b) fixed orifice's diameters.

Acknowledgements This work was supported by the National Natural Science Foundation of China (Grant No. 51975275), the National Key Laboratory of Science and Technology on Helicopter Transmission (Nanjing University of Aeronautics and Astronautics), China (Grant No. HTL-A-20G02), and the Postgraduate Research and Practice Innovation Program of Jiangsu Province, China (Grant No. KYCX20_0178).

References

1. Yang H Y, Pan M. Engineering reseasrch in fluid power: A review. Journal of Zhejiang University. Science A, 2015, 16(6): 427–442
2. Vukovic M, Murrenhoff H. The next generation of fluid power systems. Procedia Engineering, 2015, 106: 2–7
3. Scheidl R, Linjama M, Schmidt S. Is the future of fluid power digital. Proceedings of the Institution of Mechanical Engineers. Part I, Journal of Systems and Control Engineering, 2012, 226(6): 721–723
4. Pan M, Plummer A. Digital switched hydraulics. Frontiers of Mechanical Engineering, 2018, 13(2): 225–231
5. Brandstetter R, Deubel T, Scheidl R, et al. Digital hydraulics and "Industrie 4.0". Proceedings of the Institution of Mechanical Engineers. Part I, Journal of Systems and Control Engineering, 2017, 231(2): 82–93
6. Li J, Ding M, Yong W, et al. Evaluation and optimization of the nonlinear flow controllability of switch valve in vehicle electro-hydraulic brake system. IEEE Access: Practical Innovations, Open Solutions, 2018, 6: 31281–31293
7. Wang F, Gu L, Chen Y. A continuously variable hydraulic pressure converter based on high-speed on–off valves. Mechatronics, 2011, 21(8): 1298–1308
8. Paloniitty M, Linjama M. A miniature on/off valve concept for high performance water hydraulics. In: Proceedings of ASME/BATH 2017 Symposium on Fluid Power and Motion Control. Sarasota: ASME, 2017, V001T01A025
9. Wu S, Zhao X Y, Li C F, et al. Multi-objective optimization of a hollow plunger type solenoid for high speed on/off valve. IEEE Transactions on Industrial Electronics, 2018, 65(4): 3115–3124
10. Zhang B, Zhong Q, Ma J, et al. Self-correcting PWM control for dynamic performance preservation in high speed on/off valve. Mechatronics, 2018, 55: 141–150
11. Zhou C, Duan J, Deng G L, et al. A novel high-speed jet dispenser driven by double piezoelectric stacks. IEEE Transactions on Industrial Electronics, 2017, 64(1): 412–419
12. Hill M, Rizzello G, Seelecke S. Development and experimental characterization of a pneumatic valve actuated by a dielectric elastomer membrane. Smart Materials and Structures, 2017, 26(8): 085023
13. Xue G, Zhang P, He Z, et al. Displacement model and driving voltage optimization for a giant magnetostrictive actuator used on a high-pressure common-rail injector. Materials & Design, 2016, 95: 501–509
14. Winkler B, Ploeckinger A, Scheidl R. A novel piloted fast switching multi poppet valve. International Journal of Fluid Power, 2010, 11(3): 7–14
15. Wang F, Gu L Y, Chen Y. A hydraulic pressure-boost system based on high-speed on–off valves. IEEE/ASME Transactions on Mechatronics, 2013, 18(2): 733–743
16. Laamanen A, Linjama M, Tammisto J, et al. Velocity control of water hydraulic motor. Proceedings of the Fifth JFPS International Symposium on Fluid Power, 2002, 2002(5–1): 167–172
17. Laamanen A, Siivonen L, Linjama M, et al. Digital flow control unit-an alternative for a proportional valve. In: Proceedings of Bath Workshop on Power Transmission and Motion Control. Professional Engineering Publishing, 2004, 297
18. Heikkilä M, Linjama M. Displacement control of a mobile crane using a digital hydraulic power management system. Mechatronics, 2013, 23(4): 452–461
19. Lantela T, Pietola M. High-flow rate miniature digital valve system. International Journal of Fluid Power, 2017, 18(3): 188–195
20. Tamburrano P, Plummer A, De Palma P, et al. A novel servo valve pilot stage actuated by a piezoelectric ring bender (Part II): Design Model and Full Simulation. Energies, 2020, 13(9): 2267
21. Zeng Y S, Wang D, Zi B, et al. Dynamic characteristics of priority control system for high-speed on–off digital valve. Advances in Mechanical Engineering, 2015, 7(4): 1–8
22. Wang S, Zhang B, Zhong Q, et al. Study on control performance of pilot high-speed switching valve. Advances in Mechanical Engineering, 2017, 9(7): 664–671
23. Xiong X Y, Huang J H. Performance of a flow control valve with pilot switching valve. Proceedings of the Institution of Mechanical Engineers. Part I, Journal of Systems and Control Engineering, 2018, 232(2): 178–194
24. Huang J H, Wang X N, Wang H, et al. Development of a flow control valve with digital flow compensator. Flow Measurement and Instrumentation, 2019, 66: 157–169
25. Zhang J, Lu Z, Xu B, et al. Investigation on the dynamic characteristics and control accuracy of a novel proportional directional valve with independently controlled pilot stage. ISA Transactions, 2019, 93: 218–230
26. Xu B, Su Q, Zhang J H, et al. Analysis and compensation for the cascade dead-zones in the proportional control valve. ISA Transactions, 2017, 66: 393–403
27. Merritt H E. Hydraulic Control Systems. Beijing: Science Press, 1978, 97–104 (in Chinese)
28. Gao Q, Zhu Y C, Luo Z, et al. Investigation on adaptive pulse width modulation control for high speed on off valve. Journal of Mechanical Science and Technology, 2020, 34(4): 1711–1722
29. Yao J Y, Deng W, Jiao Z X. Adaptive control of hydraulic actuators with LuGre model-based friction compensation. IEEE Transactions on Industrial Electronics, 2015, 62(10): 6469–6477
30. Wang Y, Semlitsch B, Mihaescu M, et al. Flow induced energy losses in the exhaust port of an internal combustion engine. Journal of Fluids Engineering, 2015, 137(1): 011105
31. Semlitsch B, Wang Y, Mihăescu M. Flow effects due to valve and piston motion in an internal combustion engine exhaust port. Energy Conversion and Management, 2015, 96: 18–30